applied sciences

MDPI

Review

Noise Measurement and Reduction in Mode-Locked Lasers: Fundamentals for Low-Noise Optical Frequency Combs

Haochen Tian *, Youjian Song and Minglie Hu

Ultrafast Laser Laboratory, Key Laboratory of Opto-Electronic Information Technical Science of Ministry of Education, School of Precision Instrument and Opto-Electronics Engineering, Tianjin University, Tianjin 300072, China; yjsong@tju.edu.cn (Y.S.); huminglie@tju.edu.cn (M.H.)
* Correspondence: haochentian@tju.edu.cn

Abstract: After five decades of development, mode-locked lasers have become significant building blocks for many optical systems in scientific research, industry, and biomedicine. Advances in noise measurement and reduction are motivated for both shedding new light on the fundamentals of realizing ultra-low-noise optical frequency combs and their extension to potential applications for standards, metrology, clock comparison, and so on. In this review, the theoretical models of noise in mode-locked lasers are first described. Then, the recent techniques for timing jitter, carrier-envelope phase noise, and comb-line noise measurement and their stabilization are summarized. Finally, the potential of the discussed technology to be fulfilled in novel optical frequency combs, such as electro-optic (EO) modulated combs, microcombs, and quantum cascade laser (QCL) combs, is envisioned.

Keywords: mode-locked laser; noise measurement; optical frequency comb

Citation: Tian, H.; Song, Y.; Hu, M. Noise Measurement and Reduction in Mode-Locked Lasers: Fundamentals for Low-Noise Optical Frequency Combs. *Appl. Sci.* **2021**, *11*, 7650. https://doi.org/10.3390/app11167650

Academic Editor: Guillaume Duchateau

Received: 8 July 2021
Accepted: 16 August 2021
Published: 20 August 2021

1. Introduction

Mode-locked lasers have attracted growing interest since their first emergence, benefiting from their superior features of an ultra-broad optical spectrum, ultra-short pulse duration, and ultra-high peak power in output pulses. They have widely acted as laser sources in various scenarios e.g., time-resolved pump-probe experiments [1], imaging [2–5], and light-matter interactions [6]. In particular, insight into the frequency-domain picture of optical pulse trains enables femtosecond mode-locked lasers to be the most powerful optical sources for generating low-noise, phase-stabilized optical frequency combs (OFCs) with discrete, equally spaced, low-noise comb teeth. Since the 2000s, the frequency-comb concept has created novel frequency-domain spectroscopy [7,8] as well as gear work in optical atomic clocks by coherently linking optical and microwave frequencies [9,10]. Then, advances in optical frequency combs pushed mode-locked-laser-based metrology to an unprecedented level. Low-noise OFCs play essential roles in a wide variety of high-precision applications, such as distance ranging [11–13], dual-comb spectroscopy [14–16], and ultra-low-noise microwave generation [17,18], among others.

Phase stabilization of optical modes is an essential pre-requisite for the establishment of low-noise OFCs and their extended applications. Frequencies of individual comb teeth in OFCs from mode-locked lasers are defined by the comb equation, $\nu_n = n \times f_{rep} + f_{ceo}$, where ν_n is the optical frequency of the individual comb tooth, n is the integer number, f_{rep} is the repetition rate that describes the separation of comb teeth, and f_{ceo} is the carrier-envelope offset frequency of the comb. This basic equation leads to the measurement and reduction of two types of fundamental noises. Noise in the repetition rate corresponds to timing jitter of optical pulses. Optical pulses with low timing jitter are vital in many scenarios while serving as accurate timing references. For example, low-timing-jitter laser sources are a pre-requisite for the long-distance transfer of high-precision timing

standards [19,20]. An accurate long-distance timing-standard transfer is crucial in large-scale scientific instruments, such as the synchronous laser-microwave networks in X-ray free-electron lasers [21] and coherent aperture synthesis [22]. In addition, femtosecond lasers with low timing jitter are also significant laser sources for high-precision optical sampling and photonic analog-to-digital converters [23], photonic radar [24], and optical interconnections [25].

The stability of the pulse envelope's electric field phase is also important when the pulse duration is approaching or even shorter than a single optical cycle [26]. Therefore, carrier-envelope phase stabilization is essential in applications such as coherent beam combination [27,28], multi-channel coherent pulse synthesis to generate few-cycle pulses [29–31], and arbitrary waveform generation [32]. Meanwhile, in extreme X-ray pulse generation [33–35], attosecond metrology [36], and extreme nonlinear optics [37], the phase stability of femtosecond pulses also plays a vital role. Optical pulses with a stable carrier-envelope phase can also be utilized as practical measurement tools. In 2016, Feng et al. inserted an electro-optic crystal in a Ti:sapphire femtosecond laser cavity and measured the Kerr constant of the electro-optic crystal by monitoring the change of the laser's carrier-envelope offset frequency [38]. Later, Rustige et al. realized the measurement of the Doppler effect of the intracavity pulse [39].

For the above reasons, noise measurement and reduction in mode-locked lasers are extremely essential for various applications. In this review, these are investigated from the aspect of repetition rate, carrier-envelope phase, and comb-line noise.

The rest of this review is organized as follows. In Section 2, theoretical models describing timing jitter, carrier-envelope phase noise, and comb-line noise in mode-locked lasers are provided. Detailed noise measurement and reduction methods for the three above-mentioned types of noise are introduced in Section 3. Finally, in Section 4, a selection of near-future trends and prospects for noise reduction in novel mode-locked lasers are envisioned.

2. Theoretical Models

2.1. Timing Jitter

Timing jitter in a mode-locked laser is defined as the short-term jitter of the pulse train's envelope. From the perspective of the frequency domain, timing jitter is equivalent to the repetition rate's frequency noise. The timing jitter of an optical pulse train could be introduced by various noise sources, e.g., intra-cavity amplified spontaneous emission (*ASE*), cavity's non-zero dispersion, intensity fluctuation, and recover time of the saturable absorber. The very first theoretical models depicting mode-locked lasers' timing jitter is developed by Haus and Mecozzi [40]. Through applying soliton perturbation theory to solve the perturbed master equation, the pulse train's timing jitter, governed by various noise sources are determined analytically. For soliton-pulse lasers, the timing jitter's power spectral density (PSD) from the direct coupling of intra-cavity's *ASE* could be obtained as follows:

$$S_{\Delta t}^{ASE,QL}(f) = \frac{D_T}{(2\pi f)^2}$$

$$D_T = \frac{\pi^2 \tau^2}{6E_p} \Theta \frac{2g}{T_{rt}} h\nu_0$$

where f is the Fourier frequency; D_T is the diffusion constants of *ASE*-induced group velocity for soliton pulses; τ is pulsewidth; E_p is the pulse energy; Θ is the excess spontaneous emission factor; g is the gain of the cavity; T_{rt} is the round-trip time of the optical pulse in the cavity; $h\nu_0$ is the single pulse energy. For soliton-pulse lasers, the center frequency

fluctuation can also introduce timing jitter via non-zero intra-cavity dispersion. This is called Gorden-Haus timing jitter. The PSD of Gorden-Haus timing jitter can be obtained as:

$$S_{\Delta t}^{GH}(f) = \frac{4D^2 f_{rep}^2 D_\omega}{(2\pi f)^2\left[(2\pi f)^2 + \tau_{\omega c}^{-2}\right]}$$

$$D_\omega = \frac{2}{3E_p\tau^2}\Theta\frac{2g}{T_{rt}}hv_0$$

$$\frac{1}{\tau_{\omega c}} = \frac{4}{3}\frac{g}{T_{rt}\Delta f_g^2\tau^2}$$

where D is half of the net cavity dispersion; f_{rep} is the repetition rate of the optical pulse train; D_ω is the diffusion constants of center frequency changes; $\tau_{\omega c}$ is the decay time for frequency perturbation; Δf_g is the gain bandwidth in the unit of frequency. It should be noted that the above expressions only hold for soliton-pulse lasers. For stretched-pulse lasers, more detailed perturbation formalism was developed by Namiki and Haus in 1997 [41].

The numerical model of the coupling between intensity noise and timing jitter was derived by Paschotta [42,43]. Intensity noise-induced timing jitter through self-steepening effect can be expressed as follows:

$$S_{\Delta t}^{RIN-SS} = \left(\frac{\varphi_{NL}}{2\pi^2 f T_{rt} v_0}\right)^2 S_{RIN}(f)$$

where $S_{RIN}(f)$ is the PSD of relative intensity noise; φ_{NL} is the round-trip nonlinear phase shift; ν_0 is the optical frequency of the pulse. Intensity noise-induced timing jitter through Kramers-Krönig relation can be expressed as:

$$S_{\Delta t}^{RIN-KK} = \left(\frac{1}{2\pi\Delta f_g}\right)^2 S_{RIN}(f)$$

Intensity noise-induced timing jitter through slow saturable absorber can be expressed as:

$$S_{\Delta t}^{SA} = \left(\frac{1}{2\pi f T_{rt}}\frac{\partial\Delta t}{\partial s}s\right)^2 S_{RIN}(f)$$

where s is the saturation parameter. All the above theoretical models reflect that, in order to effectively reduce the pulses' timing jitter, the practical methods include:

- Reduce the round-trip cavity loss in order to reduce the cavity gain. So that the timing jitter directly coupled from intra-cavity's *ASE* could be reduced.
- Reduce the net cavity dispersion, which means to make the laser work at a close-to-zero net dispersion regime. So that center frequency fluctuation induced Gorden-Haus timing jitter could be reduced.
- Reduce the cavity nonlinearity in order to reduce the pulses' round-trip nonlinear shift. So that intensity noise induced timing jitter through self-steepening effect can be reduced.
- Reduce the intensity noise of the pulse train. So that intensity noise induced timing jitter through self-steepening effect, Kramers-Krönig relation and slow saturable absorber can be reduced.

More importantly, several groups proved that the self-steepening effect induced timing jitter typically dominates timing jitter PSD in fiber mode-locked lasers due to their large intracavity nonlinear shift [44,45].

2.2. Comb-Line Noise and Carrier-Envelope Phase Noise

After the pulse train from a mode-locked laser is Fourier transformed, a discrete, comb-shaped spectrum can be obtained in the optical frequency domain. The frequency/phase noise of each comb modes is an important parameter to evaluate the performance of an OFC. The linewidth of comb modes is mainly affected by two noise terms: Schawlow-Townes linewidth limit and technical noise terms. In this sub-section, only the conclusive formalisms of these noise terms will be listed. A detailed derivation of the formalisms could be found in Refs. [46,47].

In 1958, A. L. Schawlow and C. H. Townes proposed the concept of the linewidth limit of electromagnetic waves oscillating in an optical cavity. They named this limit the Schawlow-Townes linewidth limit [46]. The physical origin of the Schawlow-Townes linewidth limit is the spontaneous emission in the laser cavity. However, due to the existence of other technical noise sources, in most lasers, the linewidth of the electromagnetic wave is much larger than the Schawlow-Townes linewidth limit. The expression of the linewidth limit is:

$$S_{vn}^{ASE,ST}(f) = 2\frac{f_{rep}^2}{(2\pi)^2}\left(\frac{(1+n_{sp})hv_0G}{P_{circ}}\right)$$

where, n_{sp} is the amplified spontaneous emission factor; G is the intracavity gain; P_{circ} is the intracavity pulse power.

In OFCs, the frequency noise PSD of comb modes introduced by a certain technical noise source X, can be described by the following formula [47]:

$$S_{vn}^{X} = \left(v_n - v_{fix}^{X}\right)^2 S_r^X(f)$$

where ν_n is the optical frequency of the comb modes; v_{fix}^{X} is the "fixed point" for a given parameter X; $S_r^X(f)$ is the PSD of the fractional repetition-rate fluctuations driven by the fluctuations in the parameter X, in the unit of 1/Hz. For comb modes' frequency noise generated by pump fluctuation, cavity length fluctuation (caused by environment), cavity loss fluctuation (caused by environment), and timing jitter (caused by amplified spontaneous radiation), $S_r^X(f)$ can be expressed by the following formalisms, respectively:

$$S_r^{pump}(f) = B\frac{1}{1+(f/f_{3dB})^2}S_{RINpunp}$$

$$S_r^{lengfh}(f) = \left(\frac{f_{rep}}{v_{group}^{L}}\right)^2 S_{length}(f)$$

$$S_r^{loss}(f) = B\frac{1}{1+(f/f_{3dB})^2}S_{loss}(f)$$

$$S_r^{ASE,\ \text{timing}}(f) = 2f_{rep}^2\left(\frac{(1+n_{sp})hv_0G}{P_{circ}}\right)\times\left[t_{rms}^2+\left(\frac{\beta_2}{4D_g\omega_{rms}}\right)\right]$$

where, $S_{RINpump}$ is the PSD of pump laser's intensity noise; B is the rate of repetition frequency change introduced by the pump power; f_{3dB} is the 3-dB roll-off frequency, which is typically 6 kHz for Er-doped fiber lasers; S_{length} (f) and S_{loss} (f) are the PSDs of cavity length fluctuation and cavity loss, respectively; v_{group}^{L} is the group velocity of pulse propagation in the laser cavity; β_2 is the net dispersion in the cavity; D_g is the gain dispersion, which is typically 0.065 ps for Er-fiber lasers; t_{rms} and ω_{rms} are the rms values of the pulse width and spectral width in the cavity, respectively.

Using the above formalisms, the contribution of various technical noise sources to every comb mode could be evaluated. It should be noted that the 0th frequency comb tooth is the carrier-envelope offset frequency. Thus, the carrier-envelope offset frequency noise originating from various technical noise sources can be obtained when $\nu_n = f_{\text{ceo}}$.

For comb modes in the optical range, the main origin of frequency noise is the fluctuation of the laser cavity length. However, for carrier-envelope phase noise, the case is rather complicated. Noise origin is distinct in different Fourier frequency ranges. For the Fourier frequency below 1 kHz, it is mainly introduced by the cavity loss; for the Fourier frequency range of 1 kHz to 100 kHz, it is mainly introduced by pump noise; for the Fourier frequency range higher than 100 kHz, it is mainly introduced by quantum noise generated by amplified spontaneous emission. A figure depicting the technical noise contribution to comb modes and carrier-envelope phase noise could be found in Ref. [47]. What's more, a discussion on the excess carrier-envelope phase noise in saturable absorbers was presented in the literature [48].

3. Noise Measurement and Reduction in Mode-Locked Lasers

3.1. Timing Jitter

3.1.1. Timing Jitter Measurement Methods

Compared with traditional microwave oscillators, the timing jitter of the optical pulse train emitted from mode-locked lasers shows superior low timing jitter. Thus, a high-precision, high-resolution timing jitter measurement technique is an essential prerequisite for their further applications.

Electronic methods: Date back to 1986, D. Linde firstly measured RF spectra of the pulse train's repetition rate and its high harmonics from a mode-locked laser to estimate the mode-locked lasers' timing jitter [49]. Years after that, the phase detector method was proposed. With the participation of a reference mode-locked laser, the timing jitter PSD can be retrieved from the phase error between the two repetition rates' harmonics of the laser under test (LUT) and the reference laser (REF). Timing jitter of Ti:sapphire mode-locked lasers [50] and various types of fiber mode-locked lasers [51–55] have been characterized by this technique. The aforementioned timing jitter detection method with direct optical-electric conversion progress has been well-introduced in Ref. [56].

Balanced optical cross-correlation: The bottleneck of dealing with the harmonics generated from the photodiode is that the signal-to-noise ratio (SNR) of the detected harmonic signal is restrained by the optical-electric conversion process. With the increase of input power, shot noise and amplitude modulation to phase modulation (AM-PM) conversion noise induced by nonlinearities from photodiodes during direct optical-electric conversion gradually becomes an issue, which generally limits the retrieved PSD at 10 kHz offset frequency [57]. To overcome this, a balanced optical cross-correlator (BOC) was demonstrated in 2003 in order to measure the relative timing jitter between a Ti:sapphire laser and a Cr:forsterite laser [58]. Timing jitter measurement based on the BOC technique requires two identical mode-locked lasers as well. A nonlinear crystal in the correlator converts the timing information of the two pulses into the intensity fluctuation of the sum frequency signal. In this way, timing jitter could be characterized with attosecond-level resolution. Since then, the BOC technique has been widely applied in timing jitter measurement of various types of mode-locked lasers, e.g., solid-state mode-locked lasers [59–61], fiber mode-locked lasers [62–66], and fiber amplifiers [67,68] due to its practicality. Later in 2016, Xin et al. improved the BOC technique and proposed the polarization-noise-suppressed balanced optical correlation (PNS-BOC) technique [69]. Through the insertion of a birefringence crystal before the optical correlator, the crosstalk between the pulses with orthogonal polarization states can be suppressed, leading to an improved SNR of error signals. The BOC technique can also be applied in relative timing instability analysis of twin-pulse soliton molecules and counter-propagating solitons in microcavity [70]. Recently, Song et al. probed the relative timing jitter in a closely separated stationary doublet soliton molecule produced by a Kerr-lens mode-locked Ti:sapphire laser by adopting the BOC technique [71]. An upper estimate of 60 as intramolecular timing jitter with 5 zs/$\sqrt{\text{Hz}}$ temporal resolution is achieved. The corresponding results are shown in Figure 1.

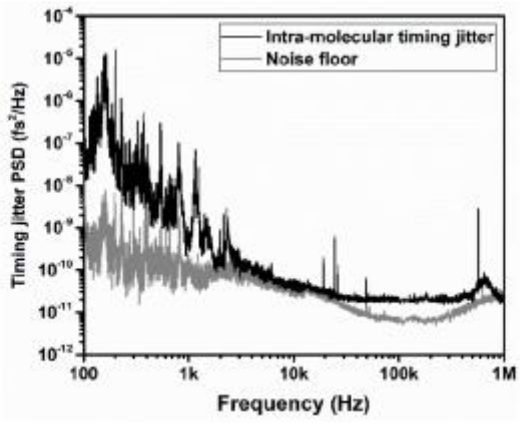

Figure 1. Timing jitter PSD of twin soliton molecule in mode-locked Ti:sapphire laser measured by BOC technique.

Optical heterodyne technique: Timing jitter measurement using optical heterodyne (OH) technique was firstly demonstrated by Hou et al. [72]. Two heterodyne beats (at the center frequency of Δf_{ceo}) at two distinct wavelengths between two independent femtosecond lasers, acting as laser under test (LUT) and reference laser (REF), are detected by two photodetectors, respectively. As shown in Figure 2a, after mixing these beats, the timing difference between two pulse trains can be converted into voltage fluctuations of the electronical signal from the RF mixer. Using this approach, the timing jitter PSD could be characterized with yoctosecond level resolution. The key point in this technique is to fully drive the mixer's LO port in order to minimize its conversion loss. Carefully using electrical amplifiers or transformers to boost up the input power is feasible. Compared with the BOC technique, the OH technique setup benefits from its ultra-high-resolution due to the two following two reasons:

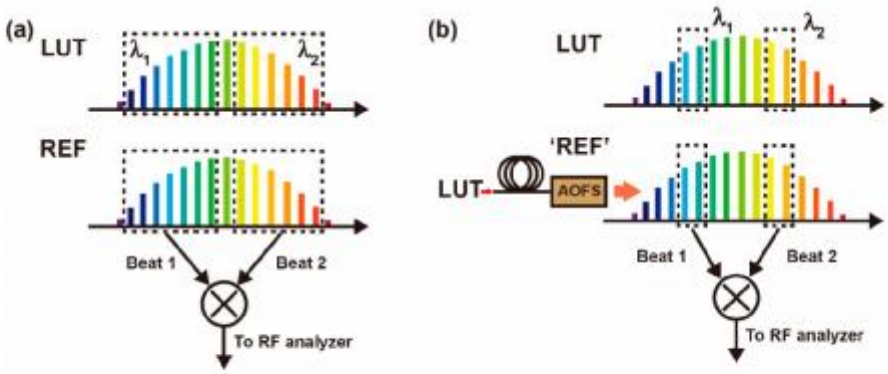

Figure 2. Experimental setup comparison of (**a**) OH technique and (**b**) DOH technique.

- In BOC setups, because of the involvement of the sum-frequency process, which is a second-order nonlinear process, the SNR of the error signal would increase as the square of the input power. In contrast, in the OH technique setup, the SNR would just simply increase as linear as the input power.
- Due to the absence of the sum-frequency process, the OH technique doesn't suffer from nonlinear conversion efficiency.

Besides timing jitter measurement of laser oscillators, the OH technique could be applied in the measurement of optical fibers' timing jitter as well [73]. Figure 3 shows a result of timing jitter PSD measurement of 5-m single-mode fiber using the OH technique. At >10 kHz Fourier frequency, the measurement is limited by electronic noise from amplifiers. At <10 kHz Fourier frequency, the PSD characterizes a slow drift with a slop of f^{-1}. The

measurement resolution is at 10^{-10} fs^2/Hz level. The integrated timing jitter is 64.7 from 10 MHz to 10 Hz.

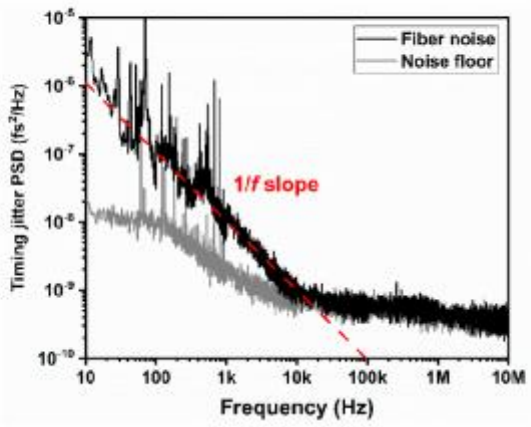

Figure 3. Timing jitter PSD of 5-m long single mode fiber using OH technique.

Delayed optical heterodyne technique: Delayed optical heterodyne (DOH) technique can be regarded as a modified version of the optical heterodyne technique. In DOH setups, a fiber delay line, and an acoustic optical frequency shifter (AOFS) are implemented to artificially create a 'reference laser' with a certain frequency offset from the laser under test (LUT), as shown in Figure 2b [74]. The fiber delay line used in this setup is typically ~100-m long that amplifies the frequency noise of the laser by a factor of τ, where τ is the delay time of the fiber. Due to the dispersion of the long fiber, the two distinct wavelengths with a narrow bandwidth (~1 nm) are required for heterodyne beats generation. In the same manner as the OH technique, after two heterodyne beats (at twice the center frequency of AOFS's driving frequency) are detected, the timing jitter PSD could be obtained through mixing these two heterodyne beats. Figure 4 shows the timing jitter PSD of a NALM Er-fiber mode-locked laser characterized by the DOH technique [45]. In this case, the measurement resolution is 10^{-7} fs^2/Hz level at 100 kHz offset frequency. For the reason that the DOH technique is capable of getting rid of reference lasers, this technique is comparatively low-cost and simple. Recently timing jitter PSD measurement of supercontinuum spectra [75], microcombs [76], monolithic fiber resonators [77] and a real-time jitter meter [78] were demonstrated by the DOH technique.

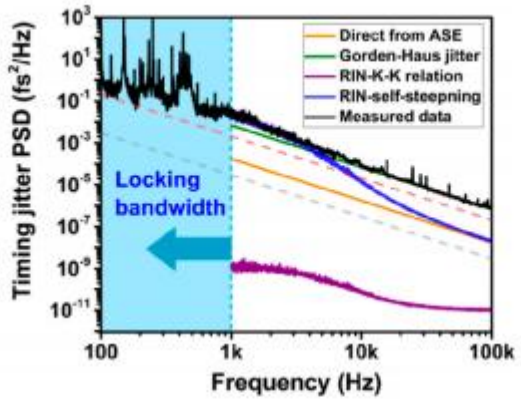

Figure 4. Timing jitter spectrum of a NALM Er-fiber mode-locked laser characterized by DOH technique. Reprint with permission from [45]. Copyright 2020 Optical Society of America.

3.1.2. Timing Jitter Reduction Methods

Intrinsic noise optimization: After the realization of high-resolution timing jitter measurement, the next interesting ongoing topic is the reduction of timing jitter of mode-locked lasers. The first type of effective method aims at the optimization of the laser oscillator's intrinsic noise. It can be seen from the theoretical models that the output pulse trains' timing jitter could be optimized through cavity loss reduction, cavity dispersion optimization, and intensity noise stabilization. In 2011, Song et al. reported the characterization of timing jitter PSDs of mode-locked lasers in soliton regime, self-similar regime, and stretched-pulse regime [64]. Furthermore, they experimentally confirmed that timing jitter PSD varies with different intracavity net dispersion. When the cavity dispersion is close to zero, the Gorden-Haus jitter is the lowest. This is consistent with the presented theoretical model in Section 2. On the other hand, by inserting a narrowband optical filter in the laser cavity, one can also reduce Gorden-Haus jitter. The main principle of this technology is that the Gorden-Haus jitter originates from the frequency fluctuation of the pulse spectrum through the cavity's non-zero net dispersion. The function of an intracavity narrow bandwidth filter is capable of partly eliminating the frequency fluctuation of the pulse spectrum, which in turn can reduce the Gorden-Haus timing jitter. Literature [79] reported for the first time that an optical filter with a bandwidth of 0.7 nm was inserted into a carbon nanotube mode-locked femtosecond laser to reduce timing jitter. In 2015, the timing jitter of femtosecond lasers with intracavity filters were studied systematically [80]. After insertion of a 7-nm narrow bandwidth optical filter in the cavity, since the Gorden-Haus jitter is largely removed, the net dispersion in the cavity has a minor impact on the timing jitter. However, if the bandwidth of the filter in the cavity is too narrow, e.g., less than 1 nm, the performance of timing the jitter will be deteriorated due to the broadening of the average pulse width in the cavity [81,82]. On the other side, reducing the pulse's intensity noise is also a feasible way. In nonlinear polarization rotation (NPR) mode-locked lasers with high repetition rates, the timing jitter at Fourier frequencies below 100 kHz is mainly introduced by intensity noise [44]. In this case, the intensity noise of the laser can be stabilized to reduce the timing jitter. In literature [83], after the intensity noise of the output pulse is reduced by pump current modulation, the timing jitter power spectrum is lowered by 10 dB in the frequency range of 3 kHz to 30 kHz.

Phase lock technology: The second type of timing jitter reduction is using phase locking technology to force the repetition rate to inherit the reference's stability. The low-noise reference sources can be atomic clocks referenced signal generators, a sapphire load resonator oscillator, or a narrow linewidth CW laser. To achieve the stabilization of the repetition rate, high bandwidth actuators are demanded to modulate the cavity length. One method is to place the end mirror of the laser cavity on a piezoelectric transducer. Through rapidly changing the voltage applied to the piezoelectric transducer, the cavity length could be modulated. The special design of the mount of the piezoelectric transducer enables the 180-kHz modulation bandwidth [84]. Recently, Nakamura et al. demonstrated a piezoelectric transducer-actuated mirror with a modulation bandwidth of 500 kHz using a simple mechanical design and electronic circuits [85]. For fiber lasers, the fiber can be wound on piezoelectric transducers. Literature [86] reported several specially designed fiber windings which enable the modulation of the repetition rate with >100 kHz bandwidth. On the other hand, inserting an electro-optic modulator in the laser cavity is also applicable. Changing the voltage applied to the electro-optic crystal changes the refractive index of the crystal, leading to a cavity length modulation above 100 kHz or even close to 1 MHz bandwidth. The shortcoming of the electro-optic modulators is that their tuning range in repetition rate is limited. In this case, piezoelectric ceramics can act as low-speed actuators with a large tuning range while electro-optical modulators act as high-speed actuators with a small tuning range. This combination enables a high-speed, long-term stable phase and reliable locking. One thing that should be noted is that the crosstalk between repetition rate modulation and carrier-envelope phase modulation would be an issue and may restrain the noise performance of fully stabilized OFCs.

3.2. Carrier-Envelope Phase Noise

3.2.1. Carrier-Envelope Phase Noise Measurement Methods

Pulse train's carrier-envelope phase performs the periodically sweeping between the pulse electric field's peak and the envelope's peak in time domain during the pulse's propagation. The carrier-envelope phase mainly accounts for the non-zero net dispersion in the femtosecond laser, which causes the difference between the pulses' group velocity and the phase velocity. The carrier-envelope phase of the femtosecond pulse is introduced by various noise sources, such as the intracavity amplified spontaneous emission, cavity loss, pump noise, and the fluctuation of the laser cavity length. In this sub-section, carrier-envelope phase noise measurement techniques are presented.

f-2f interferometry: The most used method in carrier-envelope offset frequency detection is the self-referencing based on the *f-2f* interferometer [10]. Around the 2000s, the f_{ceo} signal of Ti:Sapphire femtosecond lasers using *f-2f* interferometry was firstly reported by Jones et al., where the non-common path (NCP) *f-2f* interferometer configuration was applied. Generally speaking, the heterodyne between ν_{2n} and $2\nu_n$ components from octave-spanning supercontinuum optical spectrum results in the detection of f_{ceo}. The major issue of non-common-path configuration is that environmental fluctuations can easily introduce non-common-mode noises on both two arms of the interferometer, which will be coupled to f_{ceo}. Therefore, the establishing of a common path (CP) interferometer can eliminate non-common mode noise. In this setup, after highly nonlinear fibers (HNLF) or photonic crystal fiber (PCF), the high frequency and low-frequency parts are directed into a dispersion compensation fiber to compensate the relative group delay, ensuring that these two spectral parts overlap in the time domain. In some cases, the PPLN waveguide in the interferometer compensates for the relative group delay. CP design could eliminate the influence of non-common mode noise with all-fiber configuration, which is typically used in all-polarization-maintaining OFC systems [86]. However, the signal-to-noise ratio of the f_{ceo} signal is very sensitive to the overlap of the two frequency parts. The accuracy of cutting and splicing the dispersion compensation fiber is very restricted. Then, a quasi-common path (QCP) configuration was designed [87,88]. Based on the common path design, a dichroic mirror is used to separate the high frequency and low-frequency parts. The position of the mirror behind the dichroic mirror guarantees the two pulses' accurate time overlap. This design combines the characteristics of adjustable temporal delay and rejection of non-common noise.

The high-SNR f_{ceo} signal is significant for its stabilization. Besides the temporal overlap between ν_{2n} and $2\nu_n$ components, the coherence degradation during the generation process [89] and shot noise generated by the photodetector [90] all need to be carefully considered and optimized for high-SNR f_{ceo} detection. In addition, the use of balanced photoelectric detection can eliminate fluctuations in the amplitude of the supercontinuum spectrum to improve the signal-to-noise ratio of the f_{ceo} signal [91,92]. For the measurement of f_{ceo} PSD, the sensitivity is usually limited by the shot noise or thermal noise of the detector at 1 MHz offset frequency. The signal-to-noise ratio of the f_{ceo} signal of fiber lasers can reach 40 dB at 100 kHz resolution bandwidth [86,93–97]. For solid-state femtosecond lasers, due to their intrinsic low-noise characteristics, the signal-to-noise ratio of the f_{ceo} signal can reach 60 dB [98,99].

Active f-2f interferometry: An improved version of *f-2f* interferometer, the active *f-2f* interferometer was proposed in 2018 by Liao et al. [100]. In this setup, the 1040 nm spectral part in the *f-2f* interferometer is amplified by a Yb-fiber amplifier, as shown in Figure 5. The motivation of this setup aims to scale the frequency doubling efficiency of the 1040 nm part in the SHG crystal. This method is capable of improving the signal-to-noise ratio of f_{ceo} signal by 20 dB compared to purely passive schemes.

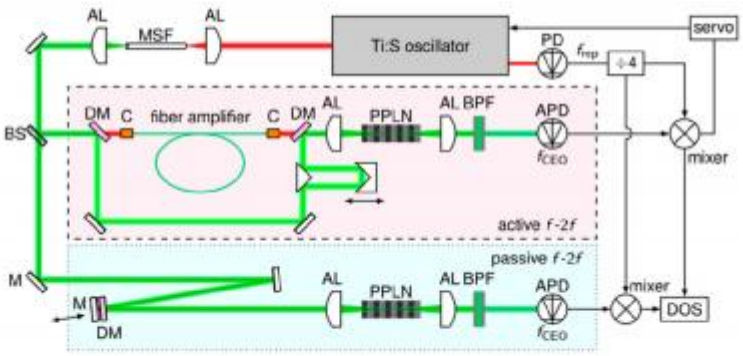

Figure 5. Setup of active *f-2f* interferometer. Reprint with permission from [100]. Copyright 2019 Optical Society of America.

Linear method: Date back to 2007, research on carrier-envelope phase detection without nonlinear process was demonstrated [101]. In this linear technique, interference between subsequent pulses from a pulse train may frustrate the interference between identical pulses, leading to a modification of interference contrast which is related to the carrier-envelope phase. Carrier-envelope phase information could be retrieved through detection of the fringe visibility. This technique allows characterizing the carrier-envelope phase with virtually arbitrarily low bandwidth and power levels.

Electrical mixing: Electrical mixing can also be applied to detect f_{ceo} signals. In 2015, Brochard et al. beat a continuous wave laser with an erbium-doped fiber femtosecond laser. Through mixing the frequency-divided beat signal with the mode-locked laser's 60th harmonic of the repetition frequency, f_{ceo} signal could be obtained [102]. Using this technique, the phase noise measurement is limited to the noise floor of the instrument when the offset frequency is higher than 100 kHz. This approach has been applied in f_{ceo} frequency noise measurement of Er:Yb:glass lasers [103] and quantum cascade lasers [104].

Time-domain detection: In addition to frequency domain detection, Kim et al. also explored a method to detect f_{ceo} signals in the time domain [105]. This method utilized the BOC technique to phase lock the repetition frequency of the laser. Interferometric cross-correlation detects the f_{ceo} signal of an erbium-doped fiber femtosecond laser in the time domain. After the error signal from the interference, cross-correlation is Fourier transformed, the power spectrum measurement of the f_{ceo} signal with an offset frequency of 2 MHz can be realized.

Optical heterodyne: f_{ceo} PSDs could also be analyzed with the participation of two mode-locked lasers. Tian et al. proposed a method to detect the relative f_{ceo} noise of two fiber lasers using the optical heterodyne method [106]. The method was based on spectral density analysis of the relative f_{ceo} beat-note obtained by direct optical heterodyning between a pair of tightly repetition-rate phase-locked OFCs. An ultra-broadband (5 mHz to 8 MHz) f_{ceo} noise spectrum with above 270 dB dynamic range was recorded and validated in passively mode-locked Yb-fiber lasers.

3.2.2. Carrier-Envelope Phase Noise Stabilization Methods

Pump power modulation: Similarly, after achieving f_{ceo} detection with high sensitivity, precise control and stabilization of the pulse trains' carrier-envelope phase pulse is an important prerequisite for obtaining a low-noise optical carrier of the femtosecond laser. Since the carrier-envelope offset frequency of the laser is mainly influenced by power fluctuation of the pump laser, in the early years, in Ti:Sapphire femtosecond laser OFCs, an acousto-optic modulator was applied to modulate the pump power. To this end, carrier-envelope offset frequency could be phase-locked to radiofrequency references [10,107–109]. Later, in the fiber femtosecond laser OFCs, pump current modulation was also applied to stabilize the carrier-envelope phase of the emitted pulse train [86,110]. However, the main bottleneck of pump power modulation in carrier-envelope phase stabilization is that the

upper-state lifetime of the gain medium in the laser will restrain the carrier-envelope phase modulation bandwidth to the order of kHz. In literature [111], through a special design of the pump current modulation circuit and optimization of the parameters of the phase-locked loop, the carrier-envelope phase lock with a bandwidth of 1 MHz was achieved.

Feedforward method: In 2010, Koke et al. proposed to use an acousto-optic frequency shifter outside the laser cavity to shift the overall frequency of the OFC to achieve the f_{ceo} modulation [112]. In this technique, f_{ceo} is modulated outside the laser cavity. Thus, the modulation bandwidth can easily reach the MHz level, determined by the acousto-optic modulator. Using the feed-forward method, they achieved a residual carrier-envelope phase noise of 45 mrad, which corresponds to a residual timing jitter of 12 as. Furthermore, by optimizing the length of the nonlinear crystal in the *f-2f* interferometer and combining with the pump power feedback modulation, they achieved a carrier-envelope phase with residual noise of 20 mrad (10 as residual timing jitter) [113]. Later in 2012, Lucking et al. demonstrated long-term carrier-envelope phase stabilization using the feed-forward method [98].

Cavity loss modulation: On the other hand, modulating the cavity loss of the laser cavity also enables modulation of f_{ceo}. Moreover, cavity loss modulation is not retrained by the gain medium's lifetime. In 2015, Kuse et al. altered the voltage on a thin piece of graphene in the erbium-doped fiber femtosecond laser to modulate the cavity loss with a high bandwidth. In this way, they demonstrated the phase-locking with a bandwidth over 1 MHz [95]. In addition, graphene-modulation-based f_{ceo} stabilization is widely used in different fiber lasers, such as all polarization-maintaining nonlinear amplification loop mirror lasers [94] and thulium-doped fiber lasers [97]. Recently, inserting an AM-EO modulator in a laser cavity to phase lock f_{ceo} through loss modulation was demonstrated by Deng et al. [114].

Phase lock to f_{rep}: The above-mentioned techniques all require a radio frequency source as a reference. Therefore, the stabilized f_{ceo} is at a certain offset frequency, which refers to that the optical phase and pulse' envelope is still periodically mismatched. To solve this issue, in 2018, Okubo et al. successfully locked the carrier-envelope offset frequency to the repetition rate [115]. Through balanced detection and dual-beat phase locking, both the $f_{rep} + f_{ceo}$ and $f_{rep} - f_{ceo}$ signals are locked to the pulse train's repetition rate. No radio references are involved and therefore electric fields under each pulse envelope are shot-to-shot reproducible.

Passively CEP-stable combs: In 2011, Krauss et al. demonstrated a passively carrier-envelope phase stabilized Er-doped fiber laser system [116]. After the output pulse of an Er-doped fiber laser system is spectrally broadened, the obtained soliton wave and the dispersion wave are sent to a different frequency generation crystal. Since the soliton wave and the dispersive wave originate from the same laser source, the f_{ceo} of the difference frequency generated pulse at 1550 nm is self-stabilized. The carrier-envelope phase noise of this system is only 250 mrad (integrated from 10 μHz to 50 MHz) [117]. Figure 6 summarizes the performance of the carrier-envelope phase noise reduction methods mentioned above.

3.3. Comb-Line Noise

3.3.1. Comb-Line Noise Measurement Methods

In Section 2, we pointed out that in mode-locked lasers, the comb-line noise, which refers to the frequency noise of optical modes, is mainly determined by the cavity length fluctuation. In this subsection, several comb-line noise measurements methods are introduced.

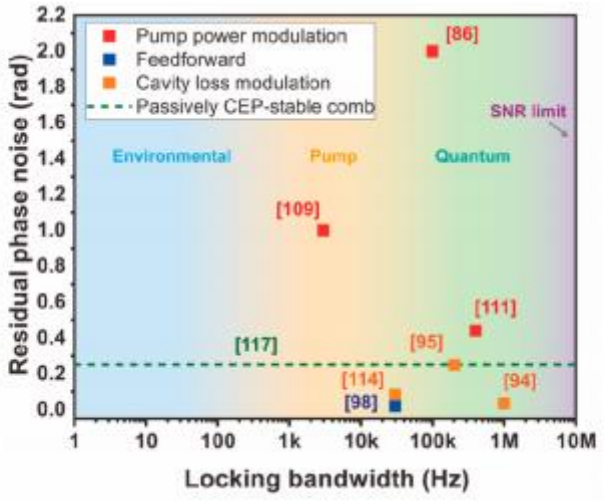

Figure 6. Representative performance of carrier-envelope phase noise reduction methods presenting as locking bandwidth vs. residual phase noise. The different color-shaded regions indicate noise of free-running comb originating from environmental noise, pump noise, quantum noise and SNR limit.

Beat with a CW laser: The most typical method to characterize the frequency noise of a certain optical mode in an OFC is to beat it with a narrow-linewidth CW laser. The use of a photodetector enables detection of the beat signal in the radio frequency range. The noise of the beat signal is related to the frequency noise of the optical comb mode when the noise of the reference CW laser is much lower than the optical modes under test. The comb-line noise power spectrum at MHz offset frequency can be obtained by this technique [86,94,95,114,118,119]. However, narrow linewidth CW lasers only exist at certain wavelengths and are not available in many wavelengths.

Asynchronous optical sampling: Early in 2007, Schlatter et al. analyzed the relative phase noise of optical modes in mode-locked lasers [120]. Their setup was based on two lasers with a slight repetition rate difference. Through numerical analysis of the asynchronous optical sampling signal, a linewidth of 50 kHz of the optical modes was measured. This approach was also capable of unraveling the correlations of the phases of different modes.

Multiple fringe-side locking method: Coluccelli et al. proposed a multiple fringe-side locking method to characterize the frequency noise spectrum of optical modes, requiring no additional reference lasers [121]. They used the transmission curve of a low finesse Fabry-Pérot cavity as a high-precision phase discriminator. The comb-line noise spectrum can be characterized up to 1 MHz offset frequency.

Delayed optical heterodyne technique: Besides the optical cavity, the fiber delay line could also serve as a sensitive phase discriminator for frequency noise measurement in OFCs. Recently, Tian et al. applied the DOH technique in an asymmetric fiber delay line interferometer to characterize the frequency noise of comb modes [45]. The delayed self-heterodyne process can magnify the frequency noise of the laser under test by a factor of τ, which is the round-trip delay time between the two arms in the interferometer. Through demodulation of the heterodyne beat note, the frequency noise spectrum of a single comb line could be retrieved, as shown in Figure 7.

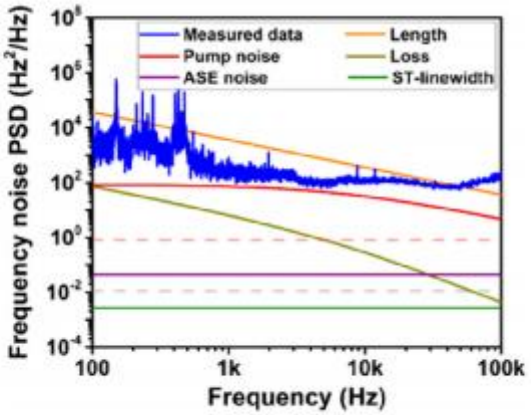

Figure 7. Comb-line noise PSD measured by DOH technique. Reprint with permission from [73]. Copyright 2020 Optical Society of America.

Correlation between n × f_{rep} noise and f_{ceo} noise: It has been reported by serval groups that, comb-line noise spectrum in OFCs is not the simple sum of their n × f_{rep} and f_{ceo} noise spectra [45,103,122,123]. There is anti-correlation between n × f_{rep} noise and f_{ceo} noise, which can be described by the following equation:

$$S_{\Delta\nu_n\Delta\nu_n} = S_{\Delta f_{ceo}\Delta f_{ceo}} + S_{N\cdot\Delta f_{rep}N\cdot\Delta f_{rep}} + \Gamma_\Delta(\omega) \times \sqrt{S_{\Delta f_{ceo}\Delta f_{ceo}} \cdot S_{N\cdot\Delta f_{rep}N\cdot\Delta f_{rep}}}$$

where $S_{\Delta\nu_n\Delta\nu_n}$, $S_{N\cdot\Delta f_{rep}N\cdot\Delta f_{rep}}$ and $S_{\Delta f_{ceo}\Delta f_{ceo}}$ are frequency noise spectra of ν_n noise, n × f_{rep} noise, and f_{ceo} noise, respectively, Γ_Δ (ω) is the sum of complex coherence. This phenomenon indicates that n × f_{rep} and f_{ceo} noise to some extent cancel out, resulting in a lower level of comb-line noise spectrum. The complex coherence was measured to be −2 in a wide range of Fourier frequency in commercial OFC from Menlosystems [123], 25-GHz Er:Yb glass lasers [103], NALM fiber mode-locked lasers [45], and mid-infrared quantum cascade lasers [104] soliton molecules [124].

The technological development in phase measuring algorithm also promotes the radio signals' phase noise analysis. In 2016, Kokuyama et al. proposed a digital phase-measuring algorithm [125]. Based on this algorithm, a phase noise analyzer with high precision could be built using a two-channel FPGA. f_{rep}, $f_{ceo,}$ and ν_n phase noise PSD of an OFC could be characterized with high precision using this home-built analyzer. Compared with commercial bulky phase noise analyzers, this phase noise analyzer is much simpler and low-cost.

3.3.2. Comb-Line Noise Stabilization

Phase lock to radio/optical references: Phase locking both the carrier-envelope offset frequency and the repetition rate frequency in an OFC to absolute radio frequency references is the most common and practical way for comb-line noise stabilization. In this manner, every comb mode is able to inherit the stability of the radio references, which is at 10^{-12}~10^{-13} level in 1 s [10,93]. However, in short-term scale, the linewidths of these OFCs are still not obviously narrowed down (at >kHz level) due to the inferior short-term stability of radio references. To obtain 'real' narrow linewidth OFCs, one can trace the comb modes to narrow-linewidth optical references. In this technique, the beat note signal between an OFC's certain comb line and an external optical frequency reference is phase-locked to a radio reference through fast cavity length feedback. Meanwhile, f_{ceo} is phase-locked to a radio reference. This method can push the residual phase error to <1 rad, linewidth to sub-mHz levels, and frequency stability down to 10^{-17} level (1 s average time) [108,126–128].

Phase lock to two optical references: On the other side, I. Coddington et al. proposed another stabilization scheme to fulfill low-noise OFC operation in 2008 [129]. In their

approach, two comb modes in an OFC are selected and phase-locked to two optical references. All the comb modes in the OFC are capable to inherit the stability of the optical references. This type of phase-stabilized OFCs, benefiting from relatively narrow linewidth, are widely served as indispensable laser sources in dual-comb spectroscopic applications e.g., spectroscopy [129], distance measurements [11], and low-noise microwave generation [130].

Phase lock to optical fiber delay lines: Optical fibers are another potential candidate of being reliable references for comb-line noise stabilization due to their superior short-term stability. Kwon et al. phase-locked individual comb mode of an OFC to the fiber delay line while f_{ceo} to a radio reference [131]. The fully stabilized OFC has sub-10^{-15}-level fractional frequency stability and 28-Hz absolute linewidth. This approach enables narrow linewidth OFCs based on an all-fiber, compact, practical photonic platform. Figure 8 summarizes the performance of the comb-line noise reduction methods mentioned above.

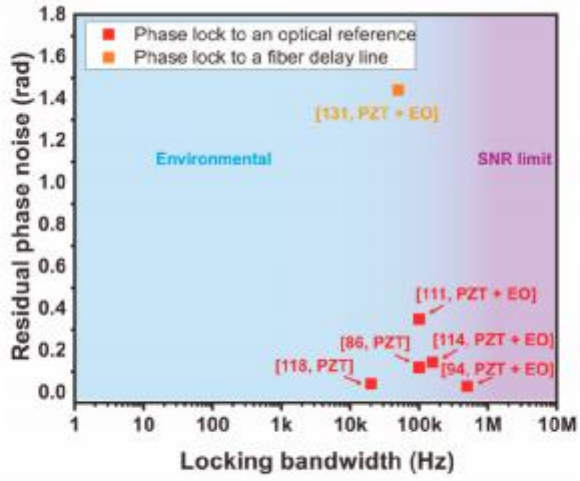

Figure 8. Representative performance of comb-line phase noise reduction methods presenting as locking bandwidth vs. residual phase noise. The different color-shaded regions indicate noise of free-running comb originating from environmental noise and SNR limit.

4. Outlook

With the rapid development of noise measurement and reduction techniques during the past two decades, optical frequency comb techniques based on traditional mode-locked lasers have gradually become mature and commercial. Thus, the general trend of advances in OFCs has headed toward high levels of integration, compactness, low power consumption, and practicality [132]. Owing to the fact that f_{ceo} stabilization is always the key technique due to the requirement of *f-2f* self-referencing, A pulse energy greater than the nJ level from optical amplifiers and coherent octave-spanning supercontinuum (SC) from HNLF or PCF are both critical in obtaining f_{ceo} signals with a >30-dB signal-to-noise ratio. The development of Si_3N_4 on-chip devices, benefiting from their high nonlinearity and engineerable dispersion, favors the advances of f_{ceo} detection toward low required pulse energy in supercontinuum generation [133–135]. Furthermore, $LiNbO_3$ waveguides enable direct f_{ceo} detection using a single waveguide with <1-nJ-level pulses. These fancy on-chip devices integrated SC generation, frequency doubling, and spectral temporal overlap compensation into a single chip, significantly simplifying the experimental setup of f_{ceo} detection [136–139].

A significant number of ongoing research topics, e.g., high-speed photonic analog-to-digital conversion [140], dual-comb spectroscopic measurements [141–147], X-band ultra-low-noise microwave generation [148–151], and astro-combs [152–155], require frequency combs with large mode spacing, therefore novel optical frequency combs aim to boost the comb spacing over the GHz level. Representative techniques generating high-

repetition-rate laser sources are QCL-based combs [156,157], microcombs [158–160], and EO-modulated combs [161,162]. The detailed study of noise behavior in these novel combs could be found in this literature [150,162–165]. However, the limited pulse energy restrains feasible f_{ceo} detection using traditional *f-2f* interferometry. Phase linking of these novel combs to fully stabilized mode-locked lasers is one feasible option to eliminate f_{ceo} locking [166–170]. On the other side, on-chip devices also enable f_{ceo} detection in EO-combs and microcombs [149,171]. From this point of view, as summarized in Table 1, most of the noise measurement techniques discussed in this review show significant potential for implementation in such novel frequency combs, opening a broader prospect for future metrological applications.

Table 1. Summary of key parameters that required for noise measurement and whether it is applicable in novel OFCs.

Noise Measurement Technique		Parameters Required in Traditional OFCs	Whether It Is Applicable in Novel OFCs
Timing jitter measurement	BOC	Peak power: >2 kW [a]	√ [b]
	OH and DOH	Average power: 20~80 mW Optical bandwidth: 20 nm	√
Carrier envelope phase noise measurement	*f-2f* interferometry based on HNLF/PCF	Pulse energy: 1 nJ [c]	× [d]
	f-2f interferometry based on waveguides	Pulse energy: 30~100 pJ	√
	Linear method, electrical mixing, OH and time domain detection	Average power: mW level [e]	√
Comb line noise measurement	Beat with CW laser	Power per comb line: nW to uW level [f]	√
	Asynchronous optical sampling, Multiple fringe-side locking method and DOH	Average power: mW level [g]	√

[a]. For Ti:sapphire lasers, the peak power is 134 kW in Ref. [59]. [b]. In Ref. [70], the authors measured the timing jitter of counter-propagating solitons in microcavity using BOC. BOC technique has not been applied in other novel combs yet, to the best of our knowledge. [c]. For Yb fiber lasers, the pulse energy is 12 nJ in Ref. [172]. For Ti: sapphire lasers, typically the pulse energy is around serval nJ. [d]. EO-comb's f_{ceo} detection based *2f-3f* interferometry using HNLF was demonstrated in Ref. [173]. [e]. In Ref. [106], the lasers' are ~80 mw. In Ref. [105], the laser's average power is 20 mW (10 pJ). [f]. Typically, obtaining a beat signal with >30 dB SNR requires about serval hundreds nW comb line power. A simple and robust technique to improve the SNR of beat signal between an OFC and a CW laser could be found in Ref. [174]. [g]. In Ref. [120], the average power is 30 mw. In Ref. [121], the average power after optical bandpass filter is 10 mw.

Author Contributions: Conceptualization, H.T. and M.H.; writing—original draft preparation, H.T.; writing—review and editing, Y.S. and M.H.; funding acquisition, M.H. All authors have read and agreed to the published version of the manuscript.

Funding: This work was supported by National Natural Science Foundation of China (618278221), Tianjin Research Program of Application Foundation and Advanced Technology of China (17JCJQJC43500) and State Key Laboratory of Advanced Optical Communication Systems and Networks, Shanghai Jiao Tong University, China (2020GZKF011).

Data Availability Statement: The data presented in this study are available on request from the corresponding author.

Acknowledgments: Haochen Tian is currently a postdoctoral researcher in the University of Electro-Communications. The authors thanks Thomas Schibli in University of Colorado for providing the equipment and supervision for fiber timing jitter measurement using OH technique.

Conflicts of Interest: The authors declare no conflict of interest.

References

1. Zewail, A.H. Femtochemistry: Atomic-Scale Dynamics of the Chemical Bond Using Ultrafast Lasers (Nobel Lecture). *Angew. Chem. Int. Ed.* **2000**, *39*, 2586–2631. [CrossRef]
2. Huang, D.; Swanson, E.A.; Lin, C.P.; Schuman, J.S.; Stinson, W.G.; Chang, W.; Hee, M.R.; Flotte, T.; Gregory, K.; Puliafito, C.A. Optical coherence tomography. *Science* **1991**, *254*, 1178–1181. [CrossRef]
3. Gao, L.; Liang, J.; Li, C.; Wang, L. Single-shot compressed ultrafast photography at one hundred billion frames per second. *Nat. Cell Biol.* **2014**, *516*, 74–77. [CrossRef]
4. Ideguchi, T.; Holzner, S.; Bernhardt, B.; Guelachvili, G.; Picqué, N.; Hänsch, T.W. Coherent Raman spectro-imaging with laser frequency combs. *Nat. Cell Biol.* **2013**, *502*, 355–358. [CrossRef] [PubMed]
5. Goda, K.; Tsia, K.K.; Jalali, B. Serial time-encoded amplified imaging for real-time observation of fast dynamic phenomena. *Nat. Cell Biol.* **2009**, *458*, 1145–1149. [CrossRef] [PubMed]
6. Gattass, R.; Mazur, E. Femtosecond laser micromachining in transparent materials. *Nat. Photon.* **2008**, *2*, 219–225. [CrossRef]
7. Hänsch, T.W. Nobel Lecture: Passion for precision. *Rev. Mod. Phys.* **2006**, *78*, 1297–1309. [CrossRef]
8. Marian, A.; Stowe, M.C.; Lawall, J.R.; Felinto, D.; Ye, J. United time-frequency spectroscopy for dynamics and global structure. *Science* **2004**, *306*, 2063–2068. [CrossRef]
9. Hall, J. Nobel Lecture: Defining and measuring optical frequencies. *Rev. Mod. Phys.* **2006**, *78*, 1279–1295. [CrossRef]
10. Jones, D.J.; Diddams, S.A.; Ranka, J.K.; Stentz, A.; Windeler, R.S.; Hall, J.L.; Cundiff, S.T. Carrier-Envelope Phase Control of Femtosecond Mode-Locked Lasers and Direct Optical Frequency Synthesis. *Science* **2000**, *288*, 635–639. [CrossRef]
11. Coddington, I.; Swann, W.C.; Nenadovic, L.; Newbury, N. Rapid and precise absolute distance measurements at long range. *Nat. Photon.* **2009**, *3*, 351–356. [CrossRef]
12. Shi, H.; Song, Y.; Li, R.; Li, Y.; Cao, H.; Tian, H.; Liu, B.; Chai, L.; Hu, M. Review of low timing jitter mode-locked fiber lasers and applications in dual-comb absolute distance measurement. *Nanotechnol. Precis. Eng.* **2018**, *1*, 205–217. [CrossRef]
13. Kim, W.; Jang, J.; Han, S.; Kim, S.; Oh, J.S.; Kim, B.S.; Kim, Y.-J.; Kim, S.-W. Absolute laser ranging by time-of-flight measurement of ultrashort light pulses. *J. Opt. Soc. Am. A* **2020**, *37*, B27–B35. [CrossRef]
14. Keilmann, F.; Gohle, C.; Holzwarth, R. Time-domain mid-infrared frequency-comb spectrometer. *Opt. Lett.* **2004**, *29*, 1542–1544. [CrossRef] [PubMed]
15. Coddington, I.; Newbury, N.; Swann, W. Dual-comb spectroscopy. *Optica* **2016**, *3*, 414–426. [CrossRef]
16. Liao, R.; Tian, H.; Liu, W.; Li, R.; Song, Y.; Hu, M. Dual-comb generation from a single laser source: Principles and spectroscopic applications towards mid-IR—A review. *J. Phys. Photon.* **2020**, *2*, 042006. [CrossRef]
17. Xie, X.; Bouchand, R.; Nicolodi, D.; Giunta, M.; Hänsel, W.; Lezius, M.; Joshi, A.; Datta, S.; Alexandre, C.; Lours, M.; et al. Photonic microwave signals with zeptosecond-level absolute timing noise. *Nat. Photon.* **2016**, *11*, 44–47. [CrossRef]
18. Nakamura, T.; Davila-Rodriguez, J.; Leopardi, H.; Sherman, J.A.; Fortier, T.M.; Xie, X.; Campbell, J.C.; McGrew, W.F.; Zhang, X.; Hassan, Y.S.; et al. Coherent optical clock down-conversion for microwave frequencies with 10−18 instability. *Science* **2020**, *368*, 889–892. [CrossRef]
19. Xin, M.; Safak, K.; Peng, M.Y.; Callahan, P.T.; Kartner, F.X. Long-term stable remote laser synchronization over a 3.5-km fiber link with one-femtosecond residual timing jitter. *Opt. Express* **2014**, *22*, 14904–14912. [CrossRef] [PubMed]
20. Tian, H.; Song, Y.; Yu, J.; Shi, H.; Hu, M. Optical–Optical Synchronization Between Two Independent Femtosecond Yb-Fiber Lasers With 10 –20 Instability in 105 s. *IEEE Photon. J.* **2017**, *9*, 1–7. [CrossRef]
21. Xin, M.; Şafak, K.; Kärtner, F.X. Ultra-precise timing and synchronization for large-scale scientific instruments. *Optica* **2018**, *5*, 1564–1578. [CrossRef]
22. Högbom, J.A. Aperture synthesis with a non-regular distribution of interferometer baselines. *Astron. Astrophys. Suppl. Ser.* **1974**, *15*, 417.
23. Khilo, A.; Spector, S.J.; Grein, M.E.; Nejadmalayeri, A.H.; Holzwarth, C.W.; Sander, M.Y.; Dahlem, M.; Peng, M.Y.; Geis, M.W.; DiLello, N.A.; et al. Photonic ADC: Overcoming the bottleneck of electronic jitter. *Opt. Express* **2012**, *20*, 4454–4469. [CrossRef]
24. Pan, S.; Zhang, Y. Microwave photonic radars. *J. Lightwave Technol.* **2020**, *38*, 5450–5484. [CrossRef]
25. Keeler, G.A.; Nelson, B.E.; Agarwal, D.; Debaes, C.; Helman, N.C.; Bhatnagar, A.; Miller, D. The benefits of ultrashort optical pulses in optically interconnected systems. *IEEE J. Sel. Top. Quantum Electron.* **2003**, *9*, 477–485. [CrossRef]
26. Brabec, T.; Krausz, F. Intense few-cycle laser fields: Frontiers of nonlinear optics. *Rev. Mod. Phys.* **2000**, *72*, 545–591. [CrossRef]
27. Klenke, A.; Müller, M.; Stark, H.; Kienel, M.; Jauregui, C.; Tünnermann, A.; Limpert, J. Coherent beam combination of ultrafast fiber lasers. *IEEE J. Sel. Top. Quantum Electron.* **2018**, *24*, 1–9. [CrossRef]
28. Tian, H.; Song, Y.; Meng, F.; Fang, Z.; Hu, M.; Wang, C. Long-term stable coherent beam combination of independent femtosecond Yb-fiber lasers. *Opt. Lett.* **2016**, *41*, 5142–5145. [CrossRef]
29. Shelton, R.K.; Ma, L.-S.; Kapteyn, H.C.; Murnane, M.M.; Hall, J.L.; Ye, J. Phase-Coherent Optical Pulse Synthesis from Separate Femtosecond Lasers. *Science* **2001**, *293*, 1286–1289. [CrossRef]
30. Krauss, G.; Lohss, S.; Hanke, T.; Sell, A.; Eggert, S.; Huber, R.; Leitenstorfer, A. Synthesis of a single cycle of light with compact erbium-doped fibre technology. *Nat. Photon.* **2009**, *4*, 33–36. [CrossRef]
31. Cox, J.A.; Putnam, W.P.; Sell, A.; Leitenstorfer, A.; Kärtner, F.X. Pulse synthesis in the single-cycle regime from independent mode-locked lasers using attosecond-precision feedback. *Opt. Lett.* **2012**, *37*, 3579–3581. [CrossRef]

32. Chan, H.-S.; Hsieh, Z.-M.; Liang, W.-H.; Kung, A.H.; Lee, C.-K.; Lai, C.-J.; Pan, R.-P.; Peng, L.-H. Synthesis and Measurement of Ultrafast Waveforms from Five Discrete Optical Harmonics. *Science* **2011**, *331*, 1165–1168. [CrossRef]
33. Drescher, M.; Hentschel, M.; Kienberger, R.; Tempea, G.; Spielmann, C.; Reider, G.A.; Corkum, P.B.; Krausz, F. X-ray Pulses Approaching the Attosecond Frontier. *Science* **2001**, *291*, 1923–1927. [CrossRef]
34. Goulielmakis, E.; Schultze, M.; Hofstetter, M.; Yakovlev, V.S.; Gagnon, J.; Uiberacker, M.; Aquila, A.L.; Gullikson, E.M.; Attwood, D.T.; Kienberger, R.; et al. Single-Cycle Nonlinear Optics. *Science* **2008**, *320*, 1614–1617. [CrossRef]
35. Gilbertson, S.; Khan, S.D.; Wu, Y.; Chini, M.; Chang, Z. Isolated Attosecond Pulse Generation without the Need to Stabilize the Carrier-Envelope Phase of Driving Lasers. *Phys. Rev. Lett.* **2010**, *105*, 093902. [CrossRef]
36. Krausz, F.; Stockman, M.I. Attosecond metrology: From electron capture to future signal processing. *Nat. Photon.* **2014**, *8*, 205–213. [CrossRef]
37. Lenzner, M.; Schnurer, M.; Spielmann, C.; Krausz, F. Extreme nonlinear optics with few-cycle laser pulses. *IEICE Trans. Electron.* **1998**, *81*, 112–122.
38. Feng, T.; Rustige, P.; Raabe, N.; Steinmeyer, G. Intracavity measurement of the electro-optic Kerr effect via carrier-envelope phase demodulation. *Opt. Lett.* **2016**, *41*, 5158–5161. [CrossRef]
39. Rustige, P.; Feng, T.; Steinmeyer, G. Influence of the Doppler effect of a periodically moving mirror on the carrier-envelope frequency of a pulse train. *Opt. Lett.* **2019**, *44*, 5246–5249. [CrossRef] [PubMed]
40. Haus, H.A.; Mecozzi, A. Noise of mode-locked lasers. *IEEE J. Quantum Electron.* **1993**, *29*, 983–996. [CrossRef]
41. Namiki, S.; Haus, H.A. Noise of the stretched pulse fiber laser. I. Theory. *IEEE J. Quantum Electron.* **1997**, *33*, 649–659. [CrossRef]
42. Paschotta, R. Noise of mode-locked lasers (Part I): Numerical model. *Appl. Phys. A* **2004**, *79*, 153–162. [CrossRef]
43. Paschotta, R. Noise of mode-locked lasers (Part II): Timing jitter and other fluctuations. *Appl. Phys. A* **2004**, *79*, 163–173. [CrossRef]
44. Wang, Y.; Tian, H.; Ma, Y.; Song, Y.; Zhang, Z. Timing Jitter of High Repetition Rate Mode-locked Fiber Lasers. *Opt. Lett.* **2018**, *43*, 4382–4385. [CrossRef]
45. Tian, H.; Yang, W.; Kwon, D.; Li, R.; Zhao, Y.; Kim, J.; Song, Y.; Hu, M.-L. Optical frequency comb noise spectra analysis using an asymmetric fiber delay line interferometer. *Opt. Express* **2020**, *28*, 9232–9243. [CrossRef]
46. Schawlow, A.L.; Townes, C.H. Infrared and Optical Masers. *Phys. Rev.* **1958**, *112*, 1940–1949. [CrossRef]
47. Newbury, N.R.; Swann, W.C. Low-noise fiber-laser frequency combs. *J. Opt. Soc. Am. B* **2007**, *24*, 1756–1770. [CrossRef]
48. Raabe, N.; Feng, T.; Mero, M.; Tian, H.; Song, Y.; Hänsel, W.; Holzwarth, R.; Sell, A.; Zach, A.; Steinmeyer, G. Excess carrier-envelope phase noise generation in saturable absorbers. *Opt. Lett.* **2017**, *42*, 1068–1071. [CrossRef] [PubMed]
49. Von der Linde, D. Characterization of the noise in continuously operating mode-locked lasers. *Appl. Phys. B* **1986**, *39*, 201–217. [CrossRef]
50. Scott, R.; Langrock, C.; Kolner, B. High-dynamic-range laser amplitude and phase noise measurement techniques. *IEEE J. Sel. Top. Quantum Electron.* **2001**, *7*, 641–655. [CrossRef]
51. Chen, J.; Sickler, J.W.; Ippen, E.P.; Kärtner, F.X. High repetition rate, low jitter, low intensity noise, fundamentally mode-locked 167 fs soliton Er-fiber laser. *Opt. Lett.* **2007**, *32*, 1566–1568. [CrossRef]
52. Oktem, B.; Ülgüdür, C.; Ilday, F.Ö. Soliton–similariton fibre laser. *Nat. Photon.* **2010**, *4*, 307–311. [CrossRef]
53. Ouyang, C.; Shum, P.; Wang, H.; Wong, J.H.; Wu, K.; Fu, S.; Li, R.; Kelleher, E.J.R.; Chernov, A.I.; Obraztsova, E.D. Observation of timing jitter reduction induced by spectral filtering in a fiber laser mode locked with a carbon nanotube-based saturable absorber. *Opt. Lett.* **2010**, *35*, 2320–2322. [CrossRef]
54. Byun, H.; Sander, M.Y.; Motamedi, A.; Shen, H.; Petrich, G.S.; Kolodziejski, L.A.; Ippen, E.P.; Kärtner, F.X. Compact, stable 1 GHz femtosecond Er-doped fiber lasers. *Appl. Opt.* **2010**, *49*, 5577–5582. [CrossRef] [PubMed]
55. Wu, K.; Zhang, X.; Wang, J.; Chen, J. 463-MHz fundamental mode-locked fiber laser based on few-layer MoS_2 saturable absorber. *Opt. Lett.* **2015**, *40*, 1374–1377. [CrossRef] [PubMed]
56. Kim, J.; Song, Y. Ultralow-noise mode-locked fiber lasers and frequency combs: Principles, status, and applications. *Adv. Opt. Photon.* **2016**, *8*, 465–540. [CrossRef]
57. Kim, J.; Chen, J.; Cox, J.; Kartner, F.X. Attosecond-resolution timing jitter characterization of free-running mode-locked lasers. *Opt. Lett.* **2007**, *32*, 3519–3521. [CrossRef]
58. Schibli, T.R.; Kim, J.; Kuzucu, O.; Gopinath, J.T.; Tandon, S.N.; Petrich, G.S.; Kolodziejski, L.A.; Fujimoto, J.G.; Ippen, E.P.; Kaertner, F.X. Attosecond active synchronization of passively mode-locked lasers by balanced cross correlation. *Opt. Lett.* **2003**, *28*, 947–949. [CrossRef]
59. Benedick, A.J.; Fujimoto, J.G.; Kärtner, F.X. Optical flywheels with attosecond jitter. *Nat. Photon.* **2012**, *6*, 97–100. [CrossRef]
60. Portuondo-Campa, E.; Paschotta, R.; LeComte, S. Sub-100 attosecond timing jitter from low-noise passively mode-locked solid-state laser at telecom wavelength. *Opt. Lett.* **2013**, *38*, 2650–2653. [CrossRef]
61. Yang, H.; Kim, H.; Shin, J.; Kim, C.; Choi, S.Y.; Kim, G.H.; Rotermund, F.; Kim, J. Gigahertz repetition rate, sub-femtosecond timing jitter optical pulse train directly generated from a mode-locked Yb: KYW laser. *Opt. Lett.* **2014**, *39*, 56–59. [CrossRef]
62. Song, Y.; Kim, C.; Jung, K.; Kim, H.; Kim, J. Timing jitter optimization of mode-locked Yb-fiber lasers toward the attosecond regime. *Opt. Express* **2011**, *19*, 14518–14525. [CrossRef]
63. Kim, T.K.; Song, Y.; Jung, K.; Nam, C.H.; Kim, J. Sub-femtosecond timing jitter optical pulse trains from mode-locked Er-fiber lasers. *Opt. Lett.* **2011**, *36*, 4443. [CrossRef] [PubMed]

64. Song, Y.; Jung, K.; Kim, J. Impact of pulse dynamics on timing jitter in mode-locked fiber lasers. *Opt. Lett.* **2011**, *36*, 1761–1763. [CrossRef] [PubMed]
65. Kim, C.; Jung, K.; Kieu, K.; Kim, J. Low timing jitter and intensity noise from a soliton Er-fiber laser mode-locked by a fiber taper carbon nanotube saturable absorber. *Opt. Express* **2012**, *20*, 29524–29530. [CrossRef] [PubMed]
66. Kim, C.; Bae, S.; Kieu, K.; Kim, J. Sub-femtosecond timing jitter, all-fiber, CNT-mode-locked Er-laser at telecom wavelength. *Opt. Express* **2013**, *21*, 26533–26541. [CrossRef] [PubMed]
67. Casanova, A.; D'Acremont, Q.; Santarelli, G.; Dilhaire, S.; Courjaud, A. Ultrafast amplifier additive timing jitter characterization and control. *Opt. Lett.* **2016**, *41*, 898–900. [CrossRef]
68. Löhl, F.; Arsov, V.; Felber, M.; Hacker, K.; Lorbeer, B.; Ludwig, F.; Matthiesen, K.; Müller, J.; Schlarb, H.; Schmidt, B.; et al. Influence of erbium-doped fiber amplifiers on the timing stability of optical pulse trains. In Proceedings of the Conference on Lasers and Electro-Optics, San Jose, CA, USA, 4–9 May 2008; p. CML5.
69. Xin, M.; Safak, K.; Peng, M.Y.; Kalaydzhyan, A.; Callahan, P.T.; Wang, W.; Mucke, O.D.; Kartner, F.X. Breaking the Femtosecond Barrier in Multi-Kilometer Timing Synchronization Systems. *IEEE J. Sel. Top. Quantum Electron.* **2016**, *23*, 97–108. [CrossRef]
70. Bao, C.; Suh, M.-G.; Shen, B.; Şafak, K.; Dai, A.; Wang, H.; Wu, L.; Yuan, Z.; Yang, Q.-F.; Matsko, A.B.; et al. Quantum diffusion of microcavity solitons. *Nat. Phys.* **2021**, *17*, 462–466. [CrossRef]
71. Song, Y.; Zhou, F.; Tian, H.; Hu, M.-L. Attosecond timing jitter within a temporal soliton molecule. *Optica* **2020**, *7*, 1531. [CrossRef]
72. Hou, D.; Lee, C.-C.; Yang, Z.; Schibli, T.R. Timing jitter characterization of mode-locked lasers with with <1 zs/$\sqrt{\text{Hz}}$ resolution using a simple optical heterodyne technique. *Opt. Lett.* **2015**, *40*, 2985–2988. [CrossRef] [PubMed]
73. Chen, Y.-F.; Jiang, J.; Jones, D. Remote distribution of a mode-locked pulse train with sub 40-as jitter. *Opt. Express* **2006**, *14*, 12134–12144. [CrossRef] [PubMed]
74. Jung, K.; Kim, J. All-fibre photonic signal generator for attosecond timing and ultralow-noise microwave. *Sci. Rep.* **2015**, *5*, 16250. [CrossRef]
75. Kwon, D.; Jeon, C.-G.; Shin, J.; Heo, M.-S.; Park, S.E.; Song, Y.; Kim, J. Reference-free, high-resolution measurement method of timing jitter spectra of optical frequency combs. *Sci. Rep.* **2017**, *7*, 40917. [CrossRef] [PubMed]
76. Jeong, D.; Kwon, D.; Jeon, I.; Do, I.H.; Kim, J.; Lee, H. Ultralow jitter silica microcomb. *Optica* **2020**, *7*, 1108. [CrossRef]
77. Jia, K.; Wang, X.; Kwon, D.; Wang, J.; Tsao, E.; Liu, H.; Ni, X.; Guo, J.; Yang, M.; Jiang, X.; et al. Photonic Flywheel in a Monolithic Fiber Resonator. *Phys. Rev. Lett.* **2020**, *125*, 143902. [CrossRef]
78. Olson, J.; Perlmutter, D.S.; Devore, P.T.S.; Chou, J.T. Real-time jitter correction in a photonic analog-to-digital converter. *Opt. Lett.* **2020**, *45*, 5089. [CrossRef]
79. Jiang, L.A.; Grein, M.E.; Ippen, E.P.; Mcneilage, C.; Searls, J.; Yokoyama, H. Quantum-limited noise performance of a mode-locked laser diode. *Opt. Lett.* **2002**, *27*, 49–51. [CrossRef]
80. Qin, P.; Song, Y.; Kim, H.; Shin, J.; Kwon, D.; Hu, M.; Wang, C.; Kim, J. Reduction of timing jitter and intensity noise in normal-dispersion passively mode-locked fiber lasers by narrow band-pass filtering. *Opt. Express* **2014**, *22*, 28276–28283. [CrossRef]
81. Chen, W.; Song, Y.; Jung, K.; Hu, M.; Wang, C.; Kim, J. Few-femtosecond timing jitter from a picosecond all-polarization-maintaining Yb-fiber laser. *Opt. Express* **2016**, *24*, 1347–1357. [CrossRef]
82. Qin, P.; Wang, S.; Hu, M.; Song, Y. Effective Removal of Gordon–Haus Jitter in Mode-Locked Fiber Lasers. *IEEE Photon. J.* **2017**, *10*, 1–8. [CrossRef]
83. Wang, Y.; Tian, H.; Hou, D.; Meng, F.; Ma, Y.; Xu, H.; Kärtner, F.X.; Song, Y.; Zhang, Z. Timing jitter reduction through relative intensity noise suppression in high-repetition-rate mode-locked fiber lasers. *Opt. Express* **2019**, *27*, 11273–11280. [CrossRef] [PubMed]
84. Briles, T.C.; Yost, D.C.; Cingöz, A.; Ye, J.; Schibli, T.R. Simple piezoelectric-actuated mirror with 180 kHz servo bandwidth. *Opt. Express* **2010**, *18*, 9739–9746. [CrossRef] [PubMed]
85. Nakamura, T.; Tani, S.; Ito, I.; Endo, M.; Kobayashi, Y. Piezo-electric transducer actuated mirror with a servo bandwidth beyond 500 kHz. *Opt. Express* **2020**, *28*, 16118–16125. [CrossRef] [PubMed]
86. Sinclair, L.C.; Deschênes, J.-D.; Sonderhouse, L.; Swann, W.C.; Khader, I.H.; Baumann, E.; Newbury, N.R.; Coddington, I. Invited Article: A compact optically coherent fiber frequency comb. *Rev. Sci. Instrum.* **2015**, *86*, 081301. [CrossRef] [PubMed]
87. Grebing, C.; Koke, S.; Manschwetus, B.; Steinmeyer, G. Performance comparison of interferometer topologies for carrier-envelope phase detection. *Appl. Phys. A* **2009**, *95*, 81–84. [CrossRef]
88. Endo, M.; Shoji, T.D.; Schibli, T.R. Ultralow noise optical frequency combs. *IEEE J. Sel. Top. Quantum Electron.* **2018**, *24*, 1–3. [CrossRef]
89. Dudley, J.M.; Genty, G.; Coen, S. Supercontinuum generation in photonic crystal fiber. *Rev. Mod. Phys.* **2006**, *78*, 1135–1184. [CrossRef]
90. Borchers, B.; Anderson, A.; Steinmeyer, G. On the role of shot noise in carrier-envelope phase stabilization. *Laser Photon. Rev.* **2014**, *8*, 303–315. [CrossRef]
91. Ruehl, A.; Martin, M.J.; Cossel, K.; Chen, L.; McKay, H.; Thomas, B.; Benko, C.; Dong, L.; Dudley, J.; Fermann, M.E.; et al. Ultrabroadband coherent supercontinuum frequency comb. *Phys. Rev. A* **2011**, *84*, 011806. [CrossRef]
92. Roos, P.A.; Li, X.; Pipis, J.A.; Cundiff, S.T. Solid-state carrier-envelope-phase noise measurements with intrinsically balanced detection. *Opt. Express* **2004**, *12*, 4255–4260. [CrossRef]

93. Schibli, T.R.; Minoshima, K.; Hong, F.L.; Inaba, H.; Onae, A.; Matsumoto, H.; Hartl, I.; Fermann, M.E. Frequency metrology with a turnkey all-fiber system. *Opt. Lett.* **2004**, *29*, 2467–2469. [CrossRef]
94. Kuse, N.; Jiang, J.; Lee, C.-C.; Schibli, T.R.; Fermann, M. All polarization-maintaining Er fiber-based optical frequency combs with nonlinear amplifying loop mirror. *Opt. Express* **2016**, *24*, 3095–3102. [CrossRef] [PubMed]
95. Kuse, N.; Lee, C.-C.; Jiang, J.; Mohr, C.; Schibli, T.R.; Fermann, M. Ultra-low noise all polarization-maintaining Er fiber-based optical frequency combs facilitated with a graphene modulator. *Opt. Express* **2015**, *23*, 24342–24350. [CrossRef] [PubMed]
96. Li, Y.; Kuse, N.; Rolland, A.; Stepanenko, Y.; Radzewicz, C.; Fermann, M.E. Low noise, self-referenced all polarization maintaining Ytterbium fiber laser frequency comb. *Opt. Express* **2017**, *25*, 18017–18023. [CrossRef] [PubMed]
97. Hartl, I.; Lee, C.-C.; Mohr, C.; Bethge, J.; Suzuki, S.; Fermann, M.E.; Schibli, T.R. Ultra-low phase-noise Tm-fiber frequency comb with an intra-cavity graphene electro-optic modulator. In Proceedings of the CLEO: Science and Innovations, San Jose, CA, USA, 6–11 May 2012; p. CTh1J.2.
98. Borchers, B.; Koke, S.; Husakou, A.; Herrmann, J.; Steinmeyer, G. Carrier-envelope phase stabilization with sub-10 as residual timing jitter. *Opt. Lett.* **2011**, *36*, 4146–4148. [CrossRef] [PubMed]
99. Shoji, T.D.; Xie, W.; Silverman, K.L.; Feldman, A.; Harvey, T.; Mirin, R.P.; Schibli, T.R. Ultra-low-noise monolithic mode-locked solid-state laser. *Optica* **2016**, *3*, 995–998. [CrossRef]
100. Liao, R.; Tian, H.; Feng, T.; Song, Y.; Hu, M.; Steinmeyer, G. Active f-to-2f interferometer for record-low jitter carrier-envelope phase locking. *Opt. Lett.* **2019**, *44*, 1060–1063. [CrossRef]
101. Osvay, K.; Görbe, M.; Grebing, C.; Steinmeyer, G. Bandwidth-independent linear method for detection of the carrier-envelope offset phase. *Opt. Lett.* **2007**, *32*, 3095–3097. [CrossRef]
102. Brochard, P.; Schilt, S.; Wittwer, V.J.; Südmeyer, T. Characterizing the carrier-envelope offset in an optical frequency comb without traditional f-to-2f interferometry. *Opt. Lett.* **2015**, *40*, 5522–5525. [CrossRef]
103. Brochard, P.; Wittwer, V.J.; Bilicki, S.; Resan, B.; Weingarten, K.J.; Schilt, S.; Sudmeyer, T. Frequency Noise Characterization of a 25-GHz Diode-Pumped Mode-Locked Laser With Indirect Carrier-Envelope Offset Noise Assessment. *IEEE Photon. J.* **2017**, *10*, 1–10. [CrossRef]
104. Shehzad, A.; Brochard, P.; Matthey, R.; Kapsalidis, F.; Shahmohammadi, M.; Beck, M.; Hugi, A.; Jouy, P.; Faist, J.; Südmeyer, T.; et al. Frequency noise correlation between the offset frequency and the mode spacing in a mid-infrared quantum cascade laser frequency comb. *Opt. Express* **2020**, *28*, 8200–8210. [CrossRef] [PubMed]
105. Kim, Y.-J.; Coddington, I.; Swann, W.C.; Newbury, N.; Lee, J.; Kim, S.; Kim, S.-W. Time-domain stabilization of carrier-envelope phase in femtosecond light pulses. *Opt. Express* **2014**, *22*, 11788–11796. [CrossRef]
106. Tian, H.; Raabe, N.; Song, Y.; Steinmeyer, G.; Hu, M. High-detectivity optical heterodyne method for wideband carrier-envelope phase noise analysis of laser oscillators. *Opt. Lett.* **2018**, *43*, 3108–3111. [CrossRef]
107. Corwin, K.; Thomann, I.; Dennis, T.; Fox, R.W.; Swann, W.; Curtis, E.A.; Oates, C.W.; Wilpers, G.; Bartels, A.; Gilbert, S.L.; et al. Absolute-frequency measurements with a stabilized near-infrared optical frequency comb from a Cr:forsterite laser. *Opt. Lett.* **2004**, *29*, 397–399. [CrossRef] [PubMed]
108. Bartels, A.; Oates, C.W.; Hollberg, L.; Diddams, S. Stabilization of femtosecond laser frequency combs with subhertz residual linewidths. *Opt. Lett.* **2004**, *29*, 1081–1083. [CrossRef]
109. Fortier, T.M.; Jones, D.J.; Ye, J.; Cundiff, S.T.; Windeler, R.S. Long-term carrier-envelope phase coherence. *Opt. Lett.* **2002**, *27*, 1436–1438. [CrossRef] [PubMed]
110. Washburn, B.R.; Diddams, S.; Newbury, N.; Nicholson, J.W.; Yan, M.F.; Jørgensen, C.G. Phase-locked, erbium-fiber-laser-based frequency comb in the near infrared. *Opt. Lett.* **2004**, *29*, 250–252. [CrossRef]
111. Ma, Y.; Xu, B.; Ishii, H.; Meng, F.; Nakajima, Y.; Matsushima, I.; Schibli, T.R.; Zhang, Z.; Minoshima, K. Low-noise 750 MHz spaced ytterbium fiber frequency combs. *Opt. Lett.* **2018**, *43*, 4136–4139. [CrossRef]
112. Koke, S.; Grebing, C.; Frei, H.; Anderson, A.; Assion, A.; Steinmeyer, G. Direct frequency comb synthesis with arbitrary offset and shot-noise-limited phase noise. *Nat. Photon.* **2010**, *4*, 462–465. [CrossRef]
113. Lücking, F.; Assion, A.; Apolonski, A.; Krausz, F.; Steinmeyer, G. Long-term carrier-envelope-phase-stable few-cycle pulses by use of the feed-forward method. *Opt. Lett.* **2012**, *37*, 2076–2078. [CrossRef]
114. Deng, Z.; Liu, Y.; Zhu, Z.; Luo, D.; Gu, C.; Zhou, L.; Xie, G.; Li, W. Ultra-precise optical phase-locking approach for ultralow noise frequency comb generation. *Opt. Laser Technol.* **2021**, *138*, 106906. [CrossRef]
115. Okubo, S.; Onae, A.; Nakamura, K.; Udem, T.; Inaba, H. Offset-free optical frequency comb self-referencing with an f-2f interferometer. *Optica* **2018**, *5*, 188–192. [CrossRef]
116. Krauss, G.; Fehrenbacher, D.; Brida, D.; Riek, C.; Sell, A.; Huber, R.; Leitenstorfer, A. All-passive phase locking of a compact Er:fiber laser system. *Opt. Lett.* **2011**, *36*, 540–542. [CrossRef] [PubMed]
117. Liehl, A.; Fehrenbacher, D.; Sulzer, P.; Leitenstorfer, A.; Seletskiy, D.V. Ultrabroadband out-of-loop characterization of the carrier-envelope phase noise of an offset-free Er:fiber frequency comb. *Opt. Lett.* **2017**, *42*, 2050–2053. [CrossRef] [PubMed]
118. Lesko, D.M.B.; Lind, A.J.; Hoghooghi, N.; Kowligy, A.; Timmers, H.; Sekhar, P.; Rudin, B.; Emaury, F.; Rieker, G.B.; Diddams, S.A. Fully phase-stabilized 1 GHz turnkey frequency comb at 156 μm. *OSA Contin.* **2020**, *3*, 2070. [CrossRef]
119. Xu, B.; Ma, Y.; Ishii, H.; Matsushima, I.; Zhang, Z.; Minoshima, K. Nonlinear amplification based on a tightly phase locked 750 MHz Yb:fiber frequency comb. *Appl. Phys. Lett.* **2021**, *118*, 031101. [CrossRef]

120. Schlatter, A.; Zeller, S.; Paschotta, R.; Keller, U. Simultaneous measurement of the phase noise on all optical modes of a mode-locked laser. *Appl. Phys. A* **2007**, *88*, 385–391. [CrossRef]
121. Coluccelli, N.; Cassinerio, M.; Gambetta, A.; LaPorta, P.; Galzerano, G. Frequency-noise measurements of optical frequency combs by multiple fringe-side discriminator. *Sci. Rep.* **2015**, *5*, 16338. [CrossRef]
122. Benkler, E.; Telle, H.R.; Zach, A.; Tauser, F. Circumvention of noise contributions in fiber laser based frequency combs. *Opt. Express* **2005**, *13*, 5662–5668. [CrossRef]
123. Dolgovskiy, V.; Bucalovic, N.; Thomann, P.; Schori, C.; Di Domenico, G.; Schilt, S. Cross-influence between the two servo loops of a fully stabilized Er:fiber optical frequency comb. *J. Opt. Soc. Am. B* **2012**, *29*, 2944–2957. [CrossRef]
124. Tian, H.; Zou, D.; Song, Y.; Hu, M. Power spectral density analysis of relative comb-line phase jitter in a twin-soliton molecule. *Opt. Commun.* **2021**, *488*, 126852. [CrossRef]
125. Kokuyama, W.; Nozato, H.; Ota, A.; Hattori, K. Corrigendum: Simple digital phase-measuring algorithm for low-noise heterodyne interferometry. *Meas. Sci. Technol.* **2016**, *27*, 085001. [CrossRef]
126. Nakajima, Y.; Inaba, H.; Hosaka, K.; Minoshima, K.; Onae, A.; Yasuda, M.; Kohno, T.; Kawato, S.; Kobayashi, T.; Katsuyama, T.; et al. A multi-branch, fiber-based frequency comb with millihertz-level relative linewidths using an intra-cavity electro-optic modulator. *Opt. Express* **2010**, *18*, 1667–1676. [CrossRef]
127. Schibli, T.R.; Hartl, I.; Yost, D.C.; Martin, M.J.; Marcinkevičius, A.; Fermann, M.E.; Ye, J. Optical frequency comb with submillihertz linewidth and more than 10 W average power. *Nat. Photon.* **2008**, *2*, 355–359. [CrossRef]
128. Fang, S.; Chen, H.; Wang, T.; Jiang, Y.; Bi, Z.; Ma, L. Optical frequency comb with an absolute linewidth of 0.6 Hz–1.2 Hz over an octave spectrum. *Appl. Phys. Lett.* **2013**, *102*, 231118. [CrossRef]
129. Coddington, I.; Swann, W.C.; Newbury, N. Coherent Multiheterodyne Spectroscopy Using Stabilized Optical Frequency Combs. *Phys. Rev. Lett.* **2008**, *100*, 013902. [CrossRef] [PubMed]
130. Swann, W.C.; Baumann, E.; Giorgetta, F.R.; Newbury, N. Microwave generation with low residual phase noise from a femtosecond fiber laser with an intracavity electro-optic modulator. *Opt. Express* **2011**, *19*, 24387–24395. [CrossRef]
131. Kwon, D.; Jeon, I.; Lee, W.-K.; Heo, M.-S.; Kim, J. Generation of multiple ultrastable optical frequency combs from an all-fiber photonic platform. *Sci. Adv.* **2020**, *6*, eaax4457. [CrossRef] [PubMed]
132. Manurkar, P.; Perez, E.F.; Hickstein, D.D.; Carlson, D.R.; Chiles, J.; Westly, D.A.; Baumann, E.; Diddams, S.A.; Newbury, N.R.; Srinivasan, K.; et al. Fully self-referenced frequency comb consuming 5 watts of electrical power. *OSA Contin.* **2018**, *1*, 274–282. [CrossRef]
133. Mayer, A.S.; Klenner, A.; Johnson, A.R.; Luke, K.; Lamont, M.R.E.; Okawachi, Y.; Lipson, M.; Gaeta, A.L.; Keller, U. Frequency comb offset detection using supercontinuum generation in silicon nitride waveguides. *Opt. Express* **2015**, *23*, 15440–15451. [CrossRef] [PubMed]
134. Klenner, A.; Mayer, A.S.; Johnson, A.R.; Luke, K.; Lamont, M.; Okawachi, Y.; Lipson, M.; Gaeta, A.L.; Keller, U. Gigahertz frequency comb offset stabilization based on supercontinuum generation in silicon nitride waveguides. *Opt. Express* **2016**, *24*, 11043–11053. [CrossRef] [PubMed]
135. Krüger, L.M.; Mayer, A.S.; Okawachi, Y.; Ji, X.; Klenner, A.; Johnson, A.R.; Langrock, C.; Fejer, M.M.; Lipson, M.; Gaeta, A.L.; et al. Performance scaling of a 10-GHz solid-state laser enabling self-referenced CEO frequency detection without amplification. *Opt. Express* **2020**, *28*, 12755–12770. [CrossRef] [PubMed]
136. Okawachi, Y.; Yu, M.; Cardenas, J.; Ji, X.; Klenner, A.; Lipson, M.; Gaeta, A.L. Carrier envelope offset detection via simultaneous supercontinuum and second-harmonic generation in a silicon nitride waveguide. *Opt. Lett.* **2018**, *43*, 4627–4630. [CrossRef] [PubMed]
137. Yu, M.; Desiatov, B.; Okawachi, Y.; Gaeta, A.L.; Lončar, M. Coherent Two-Octave-Spanning Supercontinuum Generation in Lithium-Niobate Waveguides. *Opt. Lett.* **2019**, *44*, 1222–1225. [CrossRef]
138. Okawachi, Y.; Yu, M.; Desiatov, B.; Kim, B.Y.; Hansson, T.; Loncar, M.; Gaeta, A.L. Chip-based self-referencing using integrated lithium niobate waveguides. *Optica* **2020**, *7*, 702–707. [CrossRef]
139. Hickstein, D.D.; Carlson, D.R.; Mundoor, H.; Khurgin, J.B.; Srinivasan, K.; Westly, D.; Kowligy, A.; Smalyukh, I.; Diddams, S.A.; Papp, S.B. Self-organized nonlinear gratings for ultrafast nanophotonics. *Nat. Photon.* **2019**, *13*, 494–499. [CrossRef]
140. Deakin, C.; Liu, Z. Dual frequency comb assisted analog-to-digital conversion. *Opt. Lett.* **2019**, *45*, 173–176. [CrossRef]
141. Link, S.M.; Maas, D.J.H.C.; Waldburger, D.; Keller, U. Dual-comb spectroscopy of water vapor with a free-running semiconductor disk laser. *Science* **2017**, *356*, 1164–1168. [CrossRef]
142. Villares, G.; Cappelli, F.; Hugi, A.; Blaser, S.; Faist, J. Dual-Comb Spectroscopy based on Quantum Cascade Laser Frequency Combs. *Nat. Commun.* **2014**, *5*, 5192. [CrossRef]
143. Trocha, P.; Karpov, M.; Ganin, D.; Pfeiffer, M.H.P.; Kordts, A.; Wolf, S.; Krockenberger, J.; Marin-Palomo, P.; Weimann, C.; Randel, S.; et al. Ultrafast optical ranging using microresonator soliton frequency combs. *Science* **2018**, *359*, 887–891. [CrossRef]
144. Dutt, A.; Joshi, C.; Ji, X.; Cardenas, J.; Okawachi, Y.; Luke, K.; Gaeta, A.L.; Lipson, M. On-chip dual-comb source for spectroscopy. *Sci. Adv.* **2018**, *4*, e1701858. [CrossRef]
145. Carlson, D.R.; Hickstein, D.D.; Cole, D.C.; Diddams, S.A.; Papp, S.B. Dual-comb interferometry via repetition rate switching of a single frequency comb. *Opt. Lett.* **2018**, *43*, 3614–3617. [CrossRef]
146. Yu, M.; Okawachi, Y.; Griffith, A.G.; Picqué, N.; Lipson, M.; Gaeta, A.L. Silicon-chip-based mid-infrared dual-comb spectroscopy. *Nat. Commun.* **2018**, *9*, 1869. [CrossRef]

147. Carlson, D.R.; Hickstein, D.D.; Papp, S.B. Broadband, electro-optic, dual-comb spectrometer for linear and nonlinear measurements. *Opt. Express* **2020**, *28*, 29148–29154. [CrossRef]
148. Kalubovilage, M.; Endo, M.; Schibli, T.R. Ultra-low phase noise microwave generation with a free-running monolithic femtosecond laser. *Opt. Express* **2020**, *28*, 25400. [CrossRef]
149. Carlson, D.R.; Hickstein, D.D.; Zhang, W.; Metcalf, A.J.; Quinlan, F.; Diddams, S.A.; Papp, S.B. Ultrafast electro-optic light with subcycle control. *Science* **2018**, *361*, 1358–1363. [CrossRef] [PubMed]
150. Lucas, E.; Brochard, P.; Bouchand, R.; Schilt, S.; Südmeyer, T.; Kippenberg, T.J. Ultralow-noise photonic microwave synthesis using a soliton microcomb-based transfer oscillator. *Nat. Commun.* **2020**, *11*, 374. [CrossRef] [PubMed]
151. Tetsumoto, T.; Nagatsuma, T.; Fermann, M.E.; Navickaite, G.; Geiselmann, M.; Rolland, A. Optically referenced 300 GHz millimetre-wave oscillator. *Nat. Photon.* **2021**, *15*, 516–522. [CrossRef]
152. McCracken, R.A.; Depagne, É.; Kuhn, R.B.; Erasmus, N.; Crause, L.A.; Reid, D.T. Wavelength calibration of a high resolution spectrograph with a partially stabilized 15-GHz astrocomb from 550 to 890 nm. *Opt. Express* **2017**, *25*, 6450. [CrossRef] [PubMed]
153. Metcalf, A.J.; Anderson, T.; Bender, C.F.; Blakeslee, S.; Brand, W.; Carlson, D.R.; Cochran, W.D.; Diddams, S.A.; Endl, M.; Fredrick, C.; et al. Stellar spectroscopy in the near-infrared with a laser frequency comb. *Optica* **2019**, *6*, 233–239. [CrossRef]
154. Obrzud, E.; Rainer, M.; Harutyunyan, A.; Anderson, M.H.; Liu, J.; Geiselmann, M.; Chazelas, B.; Kundermann, S.; LeComte, S.; Cecconi, M.; et al. A microphotonic astrocomb. *Nat. Photon.* **2018**, *13*, 31–35. [CrossRef]
155. Suh, M.-G.; Yi, X.; Lai, Y.-H.; Leifer, S.; Grudinin, I.S.; Vasisht, G.; Martin, E.C.; Fitzgerald, M.P.; Doppmann, G.; Wang, J.; et al. Searching for exoplanets using a microresonator astrocomb. *Nat. Photon.* **2018**, *13*, 25–30. [CrossRef] [PubMed]
156. Hugi, A.; Villares, G.; Blaser, S.; Liu, H.C.; Faist, J. Mid-infrared frequency comb based on a quantum cascade laser. *Nat. Cell Biol.* **2012**, *492*, 229–233. [CrossRef] [PubMed]
157. Lampin, J.-F.; Pagies, A.; Santarelli, G.; Hesler, J.; Hänsel, W.; Holzwarth, R.; Barbieri, S. Quantum cascade laser-pumped terahertz molecular lasers: Frequency noise and phase-locking using a 1560 nm frequency comb. *Opt. Express* **2020**, *28*, 2091–2106. [CrossRef]
158. Gaeta, A.L.; Lipson, M.; Kippenberg, T.J. Photonic-chip-based frequency combs. *Nat. Photon.* **2019**, *13*, 158–169. [CrossRef]
159. Nishimoto, K.; Minoshima, K.; Yasui, T.; Kuse, N. Investigation of the phase noise of a microresonator soliton comb. *Opt. Express* **2020**, *28*, 19295–19303. [CrossRef] [PubMed]
160. Wang, W.; Wang, L.; Zhang, W. Advances in soliton microcomb generation. *Adv. Photon.* **2020**, *2*, 034001. [CrossRef]
161. Kowligy, A.S.; Carlson, D.R.; Hickstein, D.D.; Timmers, H.; Lind, A.J.; Schunemann, P.G.; Papp, S.B.; Diddams, S.A. Mid-infrared frequency combs at 10 GHz. *Opt. Lett.* **2020**, *45*, 3677–3680. [CrossRef]
162. Parriaux, A.; Hammani, K.; Millot, G. Electro-optic frequency combs. *Adv. Opt. Photon.* **2020**, *12*, 223–287. [CrossRef]
163. Ishizawa, A.; Nishikawa, T.; Mizutori, A.; Takara, H.; Takada, A.; Sogawa, T.; Koga, M. Phase-noise characteristics of a 25-GHz-spaced optical frequency comb based on a phase- and intensity-modulated laser. *Opt. Express* **2013**, *21*, 29186–29194. [CrossRef] [PubMed]
164. Bartalini, S.; Borri, S.; Galli, I.; Giusfredi, G.; Mazzotti, D.; Edamura, T.; Akikusa, N.; Yamanishi, M.; De Natale, P. Measuring frequency noise and intrinsic linewidth of a room-temperature DFB quantum cascade laser. *Opt. Express* **2011**, *19*, 17996–18003. [CrossRef]
165. Bartalini, S.; Borri, S.; Cancio, P.; Castrillo, A.; Galli, I.; Giusfredi, G.; Mazzotti, D.; Gianfrani, L.; De Natale, P. Observing the Intrinsic Linewidth of a Quantum-Cascade Laser: Beyond the Schawlow-Townes Limit. *Phys. Rev. Lett.* **2010**, *104*, 083904. [CrossRef] [PubMed]
166. Kuse, N.; Schibli, T.R.; Fermann, M.E. Low noise electro-optic comb generation by fully stabilizing to a mode-locked fiber comb. *Opt. Express* **2016**, *24*, 16884–16893. [CrossRef]
167. Ishizawa, A.; Nishikawa, T.; Goto, T.; Hitachi, K.; Sogawa, T.; Gotoh, H. Ultralow-phase-noise millimetre-wave signal generator assisted with an electro-optics-modulator-based optical frequency comb. *Sci. Rep.* **2016**, *6*, 1–7. [CrossRef] [PubMed]
168. Barbieri, S.; Gellie, P.; Santarelli, G.; Ding, L.; Maineult, W.; Sirtori, C.; Colombelli, R.; Beere, H.; Ritchie, D. Phase-locking of a 2.7-THz quantum cascade laser to a mode-locked erbium-doped fibre laser. *Nat. Photon.* **2010**, *4*, 636–640. [CrossRef]
169. Argence, B.; Chanteau, B.; Lopez, O.; Nicolodi, D.; Abgrall, M.; Chardonnet, C.; Daussy, C.; Darquié, B.; Le Coq, Y.; Amy-Klein, A. Quantum cascade laser frequency stabilization at the sub-Hz level. *Nat. Photon.* **2015**, *9*, 456–460. [CrossRef]
170. Bartalini, S.; Linfield, E.H.; De Natale, P.; Consolino, L.; Nafa, M.; Cappelli, F.; Garrasi, K.; Mezzapesa, F.P.; Vitiello, M.S.; Li, L.; et al. Fully Phase Stabilized Quantum Cascade Laser Frequency Comb. *Nat. Commun.* **2019**, *10*, 2938. [CrossRef]
171. Lamb, E.; Carlson, D.; Hickstein, D.D.; Stone, J.R.; Diddams, S.; Papp, S.B. Optical-Frequency Measurements with a Kerr Microcomb and Photonic-Chip Supercontinuum. *Phys. Rev. Appl.* **2018**, *9*, 024030. [CrossRef]
172. Benko, C.; Ruehl, A.; Martin, M.J.; Eikema, K.; Fermann, M.E.; Hartl, I.; Ye, J. Full phase stabilization of a Yb:fiber femtosecond frequency comb via high-bandwidth transducers. *Opt. Lett.* **2012**, *37*, 2196–2198. [CrossRef] [PubMed]
173. Ishizawa, A.; Nishikawa, T.; Hara, K.; Hitachi, K.; Sogawa, T.; Gotoh, H. Carrier-envelope-offset locking of 25-GHz EOM comb based on a free-running CW Laser Diode. In Proceedings of the 2018 Conference on Lasers and Electro-Optics (CLEO), San Jose, CA, USA, 13–18 May 2018.
174. Deschênes, J.D.; Genest, J. Heterodyne beats between a continuous-wave laser and a frequency comb beyond the shot-noise limit of a single comb mode. *Phys. Rev. A* **2013**, *87*, 023802. [CrossRef]